DOI：10.3969/j.issn.2095-1973.2013.06.006
“卫星资料应用”专题系列

气象卫星微波湿度计资料简介

马原[1]　邹晓蕾[1,2]
（1 佛罗里达州立大学地球海洋大气科学系，美国；2 南京信息工程大学资料同化研究与应用中心，南京 210044）

第一个先进微波湿度计（AMSU-B）搭载于1998年5月13日发射的美国国家海洋与大气局（NOAA）卫星NOAA-15（http://www.wmo-sat.info/oscar/instruments/view/33）。它与第一个先进微波温度计（AMSU-A）一起分别完成对大气水汽和温度的垂直探测。与红外或可见光频段不同，微波可以穿透非降水云，因而微波湿度计可以观测到除强降水以外各种天气条件下的水汽信息。AMSU-B有5个通道，与AMSU-A的15个通道一起通称为AMSU，AMSU-B的通道1～5对应AMSU通道16～20。AMSU-B通道1～2是两个窗区通道，它们的中心频率分别位于89.9和150GHz附近，用来观测地表温度和地面发射率等参数；AMSU-B通道3～5是3个大气探测通道， 它们的中心频率分别位于（183.31±1）、（183.31±3）、（183.31±7）GHz附近的水汽吸收带，主要用来观测对流层中下层的水汽分布。AMSU-B的其他一些仪器参数见表1。

NOAA-16和NOAA-17也携带有AMSU-B，这两颗气象业务卫星的发射时间分别为2000年9月21日和2002年6月24日。从发射于2005年5月20日的NOAA-18开始，AMSU-B被微波湿度计（MHS）（http://www.wmo-sat.info/oscar/instruments/view/281）取代了。继NOAA-18发射之后， NOAA-19和欧洲共同体气象卫星计划（EUMETSAT）业务卫星MetOp-A、MetOp-B上携带的也是MHS。MetOp-A、NOAA-19、MetOp-B分别成功发射于2006年10月19日、2009年2月6日、2012年9月17日。MHS的5个通道的特点与AMSU-B的通道1～5基本相似，但中心频率和部分通道的极向略有不同。图1是用美国标准大气通过通用快速辐射传输模式（CRTM）[1]计算得到的MHS各通道星下点的权重函数的垂直分布。权重函数在某大气层的值越大，说明该层大气的辐射贡献越大。通道3～5的权重函数最大值分别位于400、600、800hPa。

中国风云三号A星（FY-3A）和B星（FY-3B）分别于2008年5月27日和2010年11月5日发射，两颗星均携带有中国自主研发的微波湿度计（MWHS）[2]。MWHS的窗区通道1和2都位于150GHz，只是极化不同；通道3～5的中心频率则与AMSU-B及MHS的对应通道非常接近（表1）。2011年10月28日发射的美国新一代卫星（Suomi NPP）上搭载的不再是MHS，而是先进技术微波探测器（ATMS）[3]。ATMS将微波温度计和微波湿度计合并在一起，是目前最先进的空载微波仪器，能够同时在位置相同而大小不同的96个视场（FOV）上提供温度和水汽资料。ATMS新增了一个对流层底层的温度通道和两个湿度通道（表1）。ATMS的通道16、17、22、20、18 分别对应MHS的通道1～5。

载有AMSU-B、MHS、MWHS和ATMS的气象卫星在轨运行时间如图2所示。AMSU-B、MHS、MWHS和ATMS 都是垂迹扫描仪器，完成每条扫描线的时间约2.67s，每条扫描线上的观测视场为90、90、98和96个不等，视场宽度都是1.1°，星下点的扫描角是0°，而最大扫描角分别为49.4°、49.4°、53.9°和52.8°。这4种微波湿度计的轨道宽度分别为2250、2250、2700和2500km，星下点的视场大小在15km左右。表1对比了这4种仪器主要特点。其中NEDT表示噪音等效温度敏感度，代表仪器噪音的大小，由表1可见MHS的NEDT最小。

Bonsignori[4]在对NOAA-18和MetOp-A MHS观测资料进行了一系列的在轨测试后，确认MHS在测量敏感性和定标精确度上都优于AMSU-B。John等[5]通过比较NOAA-16和NOAA-15、Metop-A和NOAA-17以及NOAA-19和NOAA-18这3组卫星携带的微波湿度计在星下点同时过境处（simultaneous nadir overpass，SNO）的亮温，进行了微波湿度计的卫星交叉定标。Guan等[2]通过将2010年1月FY-3A上的 MWHS与NOAA-18 MHS的观测场和模拟场之差进行对比，来检验MWHS的观测资料。研究发现，MWHS与

收稿日期：2013 年 9 月 13 日；修回日期：2013 年 11 月 8 日
第一作者：马原（1988—），Email：ym10@my.fsu.edu
通信作者：邹晓蕾，Email：xzou@fsu.edu
资助信息：全球变化研究国家重大科学研究计划（2010CB951600）

表1 AMSU-B、MHS、MWHS 和ATMS的仪器参数
Table 1 Characteristics of AMSU-B, MHS, MWHS and ATMS.

通道		中心频率（GHz）		极向（垂直V/水平H）		星下点分辨率（km）		NEDT（度）	
MHS	AMSU-B	MHS	AMSU-B	MHS	AMSU-B	MHS	AMSU-B	MHS	AMSU-B
1	1	89	89.9±0.9	V	V	15	16	0.23	0.37
2	2	157	150±0.9	V	V	15	16	0.37	0.84
3	3	183.31±1		H	V	15	16	0.55	1.06
4	4	183.31±3		H	V	15	16	0.42	0.70
5	5	190.31	183.3±7	V	V	15	16	0.35	0.60
MWHS	ATMS	MWHS	ATMS	MWHS	ATMS	MWHS	ATMS	MWHS	ATMS
1	16	150	88.2	V	V	15	33	0.90	0.30
2	17	150	165.5	H	H	15	15	0.90	0.60
3	22	183.31±1		V	H	15	15	1.10	0.90
4	20	183.31±3		V	H	15	15	0.90	0.80
5	18	183.3±7	183.31±6.6	V	H	15	15	0.90	0.80
	19	183.31±4.5			H		15		0.80
	21	183.31±1.8			H		15		0.80

NOAA-18 MHS的通道3都存在较大的暖误差，通道4～5都存在较大的冷误差。Weng等[6]指出若采用瑞利-金斯近似进行两点定标，会引进大约1K的微波湿度计观测误差。

图3中展示的是2010年的台风“Lionrock”即将登陆中国时NOAA-15、NOAA-16、NOAA-18、NOAA-19和MetOp-A以及FY-3B观测到的微波窗区通道1或2（150GHz垂直极向）的亮温分布。虽然微波可以穿透非降水云，但在台风墙和其附近的螺旋云雨带有强对流、强降水区，微波不能穿透这些降水云，再加上由于微波湿度计通道的频率高，云的散射作用较大，导致微波湿度计观测到的亮温在台风降水区剧烈下降。值得指出的是，极轨卫星一天之内飞经同一地点两次，因此如果单独使用一个先进微波湿度计，约12h才能对台风观测一次，而图3中六颗极轨卫星上的微波湿度计一起在8h之内对“Lionrock”观测了6次，相邻两次观测时间间隔最长也只有2h。我们还注意到，亮温的低值不仅出现在“Lionrock”台风主体区，也出现在其东部的一条对流云雨带上。

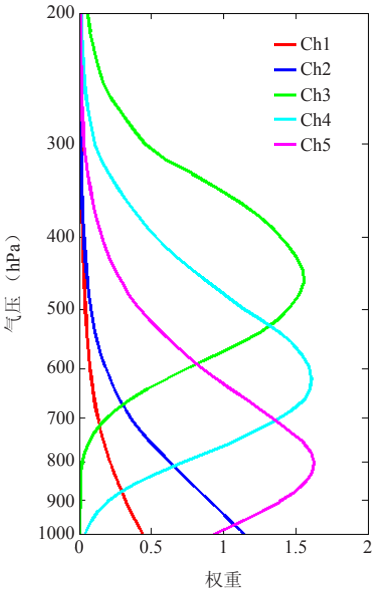

图1 NOAA-18 MHS的各个通道的权重函数
Fig. 1 weighting functions for NOAA-18 MHS channels

微波湿度计自1998年就有了，已被同化在国际上许多数值预报业务系统中。我国的数值预报系统中也用三维变分方法对微波湿度计资料进行直接同化[7]。尽管如此，怎样在数值天气预报中最有效地同化卫星微波湿度计的资料至今仍然具有很大的挑战性。McNally等[8]就曾经指出，在同化中需要考虑订正偏差、修正发射率以及检测云和降水等。由于对降水、地表过程等物理机制的观测和模拟水平都还很有限，目前怎样有效地同化对流层低层和地表通道的微波资料仍然是个挑战，具有同样难度的还有同化云区微波辐射资料。

Qin等[9]在利用美国气象局格点统计插值三维资料（GSI）同化系统进行GOES资料同化影响的研究中，发现在同化系统中引入MHS资料反而降低降水的预报评分。

GSI同化系统中MHS资料的质量控制可简述如下[10]：

首先计算随地表类型变化的云水路径经验参数（LWP_{index}）。在海洋上，LWP_{index}的计算公式为：

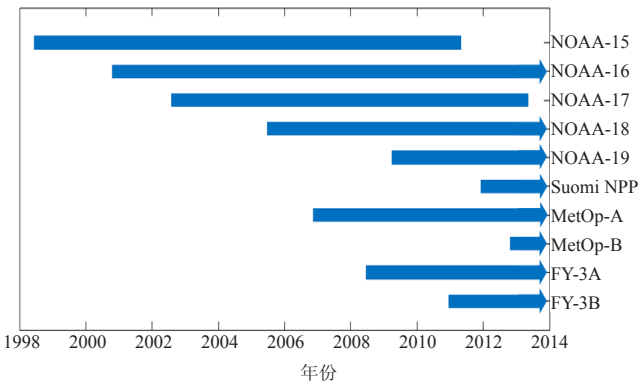

图2 载有AMSU-B、MHS、MWHS和ATMS的气象卫星的在轨时间
Fig. 2 Durations of satellites carrying AMSU-B, MHS, MWHS and ATMS

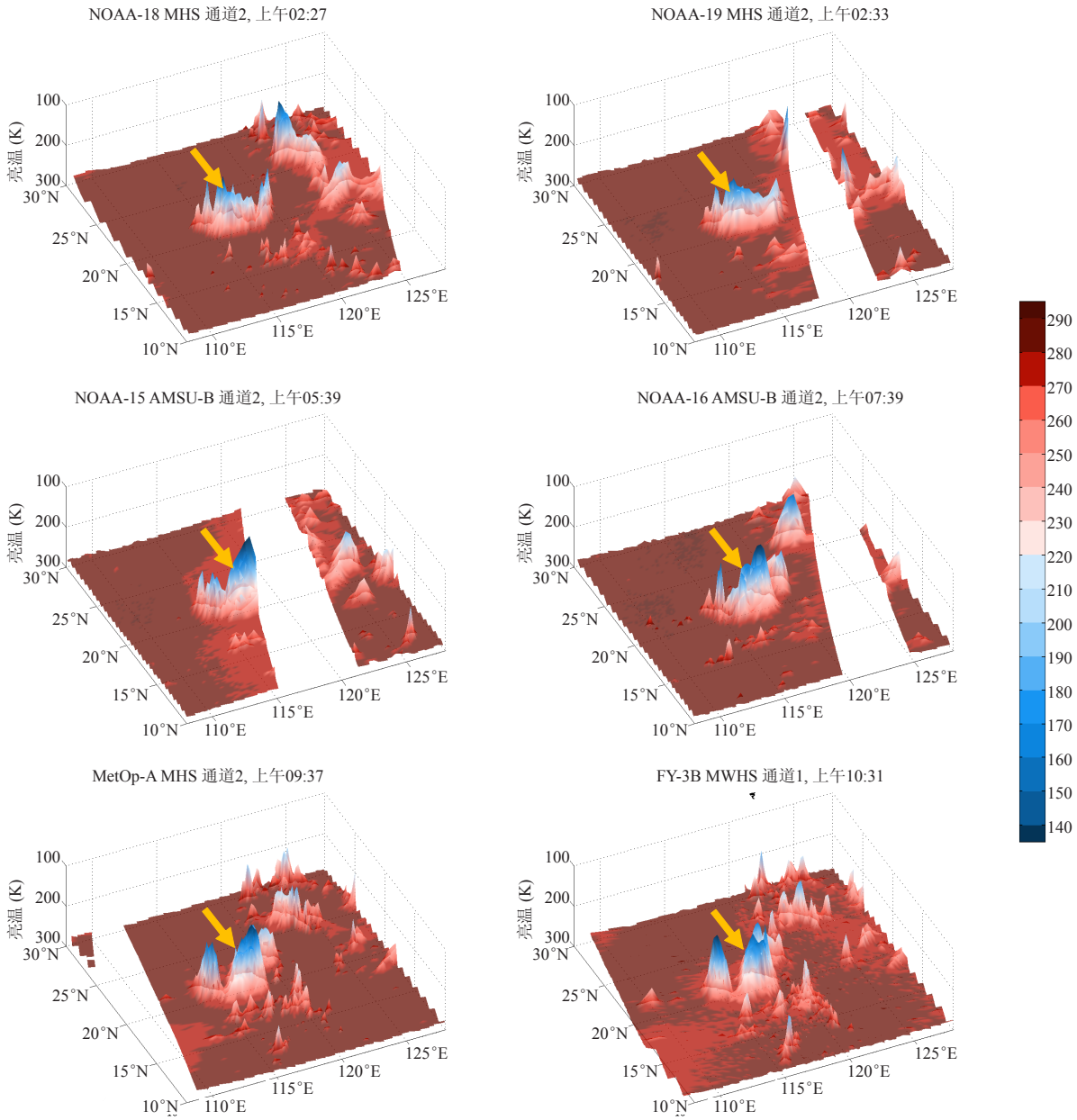

图3 NOAA–15，NOAA –16，NOAA –18，NOAA –19，MetOp–A, FY–3B观测到的2010年8月31日上午时间的微波窗区通道1或2（150GHz，V）亮温在台风“Lionrock”附近的结构。图中显示的时间均为当地时。黄色箭头指向台风主体

Fig. 3 Structures of brightness temperatures observed by NOAA–15, –16, –18, –19, MetOp–A and FY–3B at window channel 1 or 2 (150GHz, vertical polarization) on August 31st, 2010. Local time is shown. Yellow arrows point to Lionrock

$$LWP_{\text{index}}^{\text{ocean}}=\begin{cases}0.13\times[(T_{\text{b,1}}^{\text{o}}-T_{\text{b,1}}^{\text{m}})-33.58\times\dfrac{(T_{\text{b,2}}^{\text{o}}-T_{\text{b,2}}^{\text{m}})}{300-T_{\text{b,2}}^{\text{o}}}], \\ \text{若 } T_{\text{b,2}}^{\text{o}}\leqslant 300\text{K} \\ 9, \text{若 } T_{\text{b,2}}^{\text{o}}>300\text{K}\end{cases} \quad (1)$$

其中，$T_{\text{b},i}^{\text{o}}$和$T_{\text{b},i}^{\text{m}}$分别表示MHS第$i$个通道的观测亮温和模拟亮温。在陆地上，$LWP_{\text{index}}$的计算公式为：

$$LWP_{\text{index}}^{\text{land}}=0.85\times(T_{\text{b,1}}^{\text{o}}-T_{\text{b,1}}^{\text{m}})-(T_{\text{b,2}}^{\text{o}}-T_{\text{b,2}}^{\text{m}}) \quad (2)$$

GSI中MHS质量控制中的另一个参数是与单位面积总降水量有关的经验参数（TPW_{index}）：

$$TPW_{\text{index}}=\{[(T_{\text{b,1}}^{\text{o}}-T_{\text{b,1}}^{\text{m}})-7.5\times LWP_{\text{index}}]/10.0\}^2+LWP_{\text{index}}^2 \quad (3)$$

MHS质量控制的第一步，是检查总降水量经验参数值。如果某个观测点上的$TPW_{\text{index}}>1$， 就要去除该观测点上MHS所有5个通道的资料。

质量控制的第二步是检查模式和观测的差别大小。如果$\left|T_{\text{b},i}^{\text{o}}-T_{\text{b},i}^{\text{m}}\right|>3\text{e}_i^{'}$ 或者$\left|T_{\text{b},i}^{\text{o}}-T_{\text{b},i}^{\text{m}}\right|>6\text{K}$，就要去除第$i$个通道的资料，其中$\text{e}_i^{'}$是第$i$个通道调整后的观测

误差。观测误差的调整幅度与地表高度、总降水量经验参数和在大气顶层的透过率有关。具体计算公式如下：

$$e_i^{'} = e_i \times (1 - TPW_{\text{index}}^2) \times f_H \times \tau_i^{\text{top}} \quad (4)$$

其中，e_i是第i个通道的观测误差，τ_i^{top}是第i个通道在模式顶层的透过率，f_H是地表高度（H）的函数。通道1～3的观测误差为2.5K，通道4～5的观测误差为2K。如果地表高度大于2km，f_H=2000/H，否则，f_H=1 。

质量控制的第三步是检查质量控制第二步中去除的资料在通道上的一致性。即如果MHS 5个通道中的任一通道的观测资料在某个观测点在第二步中被去除，则在该观测点上的所有资料都将被剔除。

按照以上步骤，对Metop-A MHS资料进行质量控制试验。2011年12月24日世界时零时观测到的一轨结果显示在图4中。黑白背景为AVHRR可见光通道1（0.63μm）观测到的反射率，云区的反射率高，在图中显示为颜色较浅的区域。彩色为Metop-A MHS的观测点，其中红、蓝、绿分别代表步骤一、二、三中被去除的观测点，黄色代表通过了质量控制、检测为晴空的观测点。可见GSI中的质量控制过程并没能检测出一些被云污染的观测点，而另一些没有通过质量控制的观测点实际上是晴空观测点。

Zou等[10]提出在GSI系统中对MHS资料再加一个云检测步骤。他们首先建立了MHS两个窗区通道和一个最低层探测通道和GOES在10.7μm通道的成像仪资料之间的统计关系。这个统计关系如下所示：

$$(O-B)_{\text{GOES,land}}^{\text{regression}} = 0.009 \times T_{\text{b,MHS}_{\text{ch1}}}^{\text{obs}} + 0.085 \times T_{\text{b,MHS}_{\text{ch2}}}^{\text{obs}} + 0.877 \times T_{\text{b,MHS}_{\text{ch5}}}^{\text{obs}} - 274.255 \quad (5)$$

$$(O-B)_{\text{GOES,ocean}}^{\text{regression}} = -0.536 \times T_{\text{b,MHS}_{\text{ch1}}}^{\text{obs}} + 1.132 \times T_{\text{b,MHS}_{\text{ch2}}}^{\text{obs}} + 0.537 \times T_{\text{b,MHS}_{\text{ch5}}}^{\text{obs}} - 321.318 \quad (6)$$

其中，$T_{\text{b,MHS}_{\text{chi}}}^{\text{obs}}$表示MHS在第$i$个通道的观测亮温，$(O-B)_{\text{GOES}}^{\text{regression}}$表示用MHS资料得到的GOES通道4的观测亮温与模式亮温之差的线性回归函数。然后用下述条件去除被云污染的观测点：

$$(O-B)_{\text{GOES,land}}^{\text{regression}} \leqslant -4\text{K}, \quad (O-B)_{\text{GOES,ocean}}^{\text{regression}} \leqslant -2\text{K} \quad (7)$$

该算法使得GSI系统的质量控制系统可以成功检测并剔除被云污染的观测点。利用改进了的MHS资料的质量控制，再将MHS资料同化进GSI同化系统以后，降水预报评分得到显著提高。细节见Zou等[10]。

从NOAA-15、NOAA-16、NOAA-17携带的AMSU-B，到NOAA-18、NOAA-19、MetOp-A、MetOp-B携带的MHS，FY-3A、FY-3B携带的MWHS，Suomi NPP携带的ATMS（图2），这4种微波湿度计提供了超过15年的微波湿度计资料，这使得研究与水汽有关资料的气候变化成为可能。譬如，Moradi等[11]用NOAA-15、NOAA-16上的AMSU-B和NOAA-18、NOAA-19及MetOp-A上的MHS资料反演

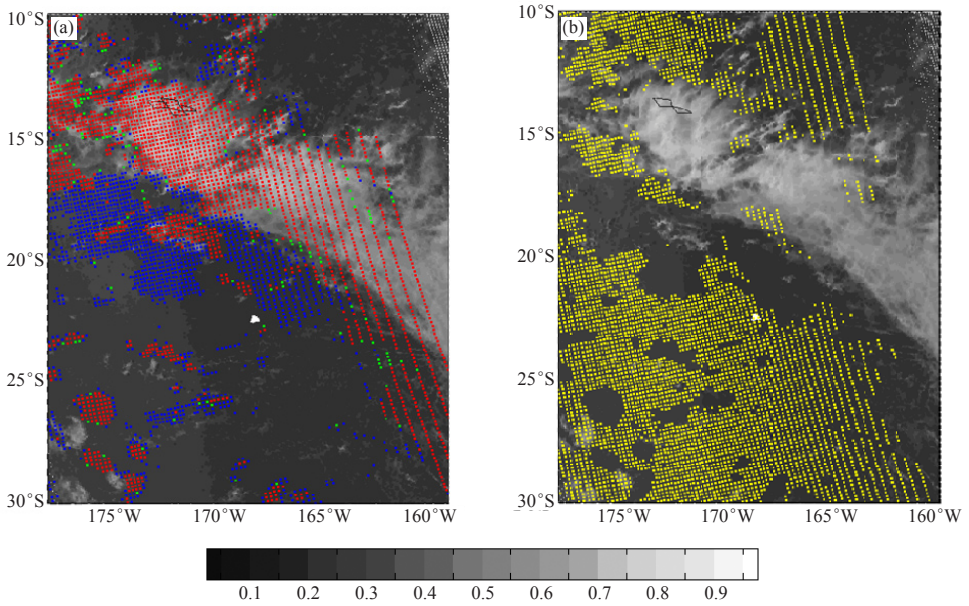

图4 根据GSI质量控制方案，（a）在第一（红）、二（蓝）、三（绿）步中分别剔除的MetOp-A MHS观测点，和（b）通过了质量控制的观测点。时间是2011年10月24日世界时零时。背景为AVHRR可见光通道1观测到的反射率

Fig. 4 (a) MetOp-A MHS data points removed in the first (red), second (blue) and third (green) QC steps according to GSI QC algorithm, the swath is at 0000 UTC, October 24 , 2011. (b) Same as (a) but for data points retained. Background is reflectivity observed at AVHRR visible channel 1

了对流层高层的水汽含量，并与无线电探空观测资料进行了对比，探讨了对流层中高层的水汽对全球大气水循环的影响。目前，微波湿度计资料在气候研究方面还没有得到广泛应用。随着微波湿度计资料长度的不断增加，该资料在与水汽相关的气候变化研究中将会有更多的应用。

Serial of Applications of Satellite Observations

An Introduction to Satellite-based Microwave Humidity Sounding Data

Ma Yuan[1], Zou Xiaolei[1, 2]

(1 Department of Earth, Ocean and Atmospheric Science, Florida State University, USA 2 Center of Data Assimilation for Research and Application, Nanjing University of Information and Science & Technology, Nanjing 210044)

With the successful launch of National Oceanic and Atmospheric Administration (NOAA) meteorological satellite NOAA-15 on May 13, 1998, the first Advanced Microwave Humidity Sounding Units-B (AMSU-B) (http://www.wmo-sat.info/oscar/instruments/view/33) came into use. AMSU-B and the first Advanced Microwave Temperature Sounding Units-A (AMSU-A) also on board NOAA-15 were designed to monitor atmospheric humidity and temperature profiles, respectively. Different from visible or infrared bands, microwave is capable of penetrating through non-precipitation clouds, and can thus operate in all-weather conditions except for heavy rainfall. Combining the five channels of AMSU-B with the 15 channels of AMSU-A gives the so-called 20 AMSU channels. In other words, AMSU channels 16-20 correspond to AMSU-B channels 1-5. The two AMSU-B window channels 1-2 have their center frequencies located at 89.9 and 150 GHz, respectively, providing measurements of surface parameters such as surface temperature and surface emissivity. The three AMSU-B sounding channels 3-5 have their central frequencies located on the 183.31 GHz vapor absorption line. Specifically, the center frequencies of AMSU-B channels 3, 4 and 5 are located at (183.31±1), (183.31±3), (183.31±7) GHz, respectively. AMSU-B channels 3-5 are designed to profile the water vapor in the troposphere. Some other channel characteristics of AMSU-B can be found in Table 1.

AMSU-B is also on board NOAA-16 and -17, which were launched on September 21, 2000 and June 24, 2002, respectively. Since the launch of NOAA-18 May 20, 2005, AMSU-B was replaced by Microwave Humidity Sounder (MHS) (http://www.wmo-sat.info/oscar/instruments/view/281). Following the launch of NOAA-18, MHS was on board NOAA-19 and the European Organization for the Exploitation of Meteorological Satellites (EUMETSAT) MetOp-A and MetOp-B, which were launched on October 19, 2006, February 6, 2009 and September 17, 2012, respectively. Channels 1-5 of MHS resemble the five channels of AMSU-B, with some minor changes in frequency allocation and polarizations. Figure 1 provides the vertical distributions of weighting functions for MHS channels calculated by the Community Radiative Transfer Model (CRTM)[1] using the US standard atmospheric profile. The larger the weighting function is at a vertical level, the larger the atmospheric contribution from that level is to the total radiation. The weighting function maxima of MHS channels 3-5 are located at 400, 600 and 800 hPa, respectively.

China also successfully launched Fengyun-3A (FY-3A) and 3B (FY-3B) on May 27, 2008 and November 5, 2010. On board FY-3A and FY-3B there is MicroWave Humidity Sounder (MWHS)[2], which was developed by China. Channels 3-5 of MWHS are similar to the three sounding channels of AMSU-B and MHS, but the two MWHS window channels 1-2 have the same center frequency of 150 GHz with different polarization states (see Table 1). The AMSU was replaced by the Advanced Technology Microwave Sounder (ATMS)[3] when the new US satellite, Suomi National Polar orbiter Partnership (NPP), was launched on October 28, 2011. ATMS combines previous microwave temperature and humidity sounders AMSU-A and MHS into a single package, and is the most advanced, state-of-the-art satellite-based microwave instrument that provides temperature and humidity information at the same 96 field-of-view (FOV) locations, although FOV sizes are different. Compared with its heritages, ATMS has included an

extra temperature channel in the low troposphere and two new humidity channels (see Table 1). ATMS channels 16, 17, 22, 20 and 18 correspond to MHS channels 1-5, respectively.

The observing time periods of the polar-orbiting satellites carrying the above-mentioned four microwave humidity sounders are provided in Fig. 2. All AMSU-B, MHS, MWHS and ATMS are cross-track, line-scanning radiometers. It takes 2.67 seconds for AMSU-B, MHS, MWHS or ATMS to complete a single scanline, with 90, 90, 98 and 96 FOVs, respectively. The beam width is 1.11°. The outmost scan-angles are 49.4°, 49.4°, 53.9° and 52.8°, and the swath widths are 2250, 2250, 2700 and 2500 km, respectively, for the four radiometers. The spatial resolution of data points are all around 15 km. Channel characteristics of those humidity sounders are compared in Table 1. NEDT represents the noise equivalent temperature sensitivity, which quantifies the magnitude of instrument noise. The NEDT for MHS is the smallest among the four microwave humidity radiometers.

Bonsignori[4] carried out an extensive satellite in-orbit verification for observations from MHS on board both NOAA-18 and MetOp-A, and concluded that the MHS data have better quality than AMSU-B in terms of data noise and calibration accuracy. John et al.[5] conducted inter-calibrations for microwave humidity sounders between three pairs of satellites, which are NOAA-16 and NOAA-15, Metop-A and NOAA-17, as well as NOAA-19 and NOAA-18. Brightness temperatures observed at simultaneous nadir overpass (SNO) were compared. FY-3A MWHS observations in January 2010 was compared with MHS data from NOAA-18 during the same period[2]. The comparison was carried out in terms of the mean and standard deviation of the differences between the observed and simulated brightness temperatures. Large positive bias at channel 3 and cold bias at channels 4-5 were found for both FY-3A MWHS and NOAA-18 MHS data and are of similar magnitudes. Weng and Zou[6] pointed out that the Rayleigh–Jeans approximation used for two-point calibration might introduce a bias as large as 1 K at MHS frequencies.

Figure 3 shows the brightness temperatures at channel 1 or 2 (150 GHz, vertical polarization) observed by NOAA-15, -16, -18, -19, MetOp-A and FY-3B, when hurricane Lionrock made landfall in China. The rapid decrease of brightness temperatures near hurricane center arises from the following two facts: (i) microwave can travel through non-precipitation clouds, but it is unable to penetrate clouds in strong convective or rainy regions such as hurricane eyewall and rainbands; (ii) radiation at high-frequency microwave humidity channels is strongly affected by scattering effects of ice clouds. Since a polar-orbiting satellite passes over a certain geographical location twice daily, any hurricane can be observed at no less than a 12-h interval by a single sounder. With microwave humidity sounders on board six satellites, however, Lionrock was observed six times during an eight-hour interval, with the longest interval between two successive observations being two hours (Fig. 3). Another interesting feature is that extremely cold brightness temperatures occur not only around Lioncock itself, but also along a convective rainband located to the east of the hurricane.

Microwave humidity sounding data have become available since 1998, and are assimilated in operational models at major Numerical Weather Prediction (NWP) centers, in China 3D-Var methods are used to directly assimilate those data[7]. However, appropriate assimilation of those data into NWP systems remains to be a great challenge even today. McNally et al.[8] once pointed out several important issues including surface emissivity adjustment, bias correction as well as cloud and precipitation detection, etc. Because of limited observations and knowledge on physical characteristics of surface processes, cloud and precipitation, assimilation of surface sensitive channels and cloud radiance are two main challenges.

Qin et al.[9] found that assimilation of MHS data in the National Center for Environmental Prediction (NCEP) Gridpoint Statistical Interpolation (GSI) system degraded the precipitation forecast scores.

Quality control (QC) procedures for MHS in GSI assimilation system is briefly introduced as follows[10].

A so-called liquid water path index (LWP_{index}) over different surface types is first calculated. Over ocean, LWP_{index} is calculated as:

$$LWP_{\text{index}}^{\text{ocean}}=\begin{cases}0.13\times[(T_{\text{b,1}}^{\text{o}}-T_{\text{b,1}}^{\text{m}})-33.58\times\dfrac{(T_{\text{b,2}}^{\text{o}}-T_{\text{b,2}}^{\text{m}})}{300-T_{\text{b,2}}^{\text{o}}}], \\ \quad\text{if } T_{\text{b,2}}^{\text{o}}\leqslant 300\text{K} \\ 9,\text{otherwise}\end{cases}, \tag{1}$$

where $T_{\text{b},i}^{\text{o}}$ and $T_{\text{b},i}^{\text{m}}$ represent observations and model simulations, respectively. Over land, the index LWP_{index} is calculated as:

$$LWP_{\text{index}}^{\text{land}}=0.85\times(T_{\text{b,1}}^{\text{o}}-T_{\text{b,1}}^{\text{m}})-(T_{\text{b,2}}^{\text{o}}-T_{\text{b,2}}^{\text{m}}). \tag{2}$$

Another index TPW_{index}, which is relevant to total-column precipitable water, is defined as:

$$TPW_{\text{index}}=\{[(T_{\text{b,1}}^{\text{o}}-T_{\text{b,1}}^{\text{m}})-7.5\times LWP_{\text{index}}]/10.0\}^2+LWP_{\text{index}}^2. \tag{3}$$

The first step of GSI QC checks magnitude of

TPW_{index}. Data from all five channels of MHS are rejected if $TPW_{\text{index}}>1$.

In the second QC step, *O-B* outliers are removed if $\left|T_{\text{b},i}^{\text{o}}-T_{\text{b},i}^{\text{m}}\right|>3\text{e}_i^{'}$ or $\left|T_{\text{b},i}^{\text{o}}-T_{\text{b},i}^{\text{m}}\right|>6\text{K}$, where i is the channel number and $\text{e}_i^{'}$ is the adjusted accuracy of observation errors, which is related to terrain height (H), TPW_{index} and transmittance at the model top (τ_i^{top}). e_i is expressed as:

$$\text{e}_i^{'}=\text{e}_i\times(1-TPW_{\text{index}}^2)\times f_H\times\tau_i^{\text{top}}, \quad (4)$$

where e_i is the accuracy of observation errors for the i^{th} channel. e_i is set to 2.5K for channels 1-3 and 2.0K for channels 4-5. f_H depends on terrain height H. If H is higher than 2 km, f_H=2000/H, otherwise f_H=1 .

The third QC step removes data from all channels if data from any of the five channels is rejected in the second step.

Based on the GSI QC algorithm described above, a Metop-A MHS QC experiment is carried out. Results of a single swath at 0000 UTC, December 24, 2011 is shown in Fig. 4. Black and white background shows the reflectivity observed at AVHRR visible channel 1 (0.63μm). Cloudy regions, which have higher reflectivity, are shown in lighter color. Metop-A MHS data points removed in the first, second and third QC steps are indicated in red, blue and green, respectively; data points retained are indicated in yellow. It is seen that GSI QC test fails to identify some cloudy data points, and it mistakenly takes some clear-sky observations as cloudy.

Zou et al.[10] developed an extra step in the GSI system for MHS cloud detection. A statistical relationship is established first, which is between observations from two MHS window channels as well as the lowest sounding channel, and observations from GOES imager channel at 10.7 μm. The statistical relationship is expressed as:

$$(O-B)_{\text{GOES,land}}^{\text{regression}}=0.009\times T_{\text{b,MHS}_{\text{ch1}}}^{\text{obs}}+0.085\times T_{\text{b,MHS}_{\text{ch2}}}^{\text{obs}}+0.877\times T_{\text{b,MHS}_{\text{ch5}}}^{\text{obs}}-274.255, \quad (5)$$

$$(O-B)_{\text{GOES,ocean}}^{\text{regression}}=-0.536\times T_{\text{b,MHS}_{\text{ch1}}}^{\text{obs}}+1.132\times T_{\text{b,MHS}_{\text{ch2}}}^{\text{obs}}+0.537\times T_{\text{b,MHS}_{\text{ch5}}}^{\text{obs}}-321.318, \quad (6)$$

where $T_{\text{b,MHS}_{\text{ch}i}}^{\text{obs}}$ indicates observed brightness temperatures at the i^{th} channel of MHS, and $(O-B)_{\text{GOES}}^{\text{regression}}$ indicates linear regression function of differences between observations and model simulations at GOES channel 4, which is calculated using MHS data. The data points satisfying the following conditions are then identified as cloudy and thus removed:

$$(O-B)_{\text{GOES,land}}^{\text{regression}}\leqslant-4\text{K},\ (O-B)_{\text{GOES,ocean}}^{\text{regression}}\leqslant-2\text{K}. \quad (7)$$

With the new algorithm added, data points contaminated by cloudy radiance were successfully identified and removed in the GSI system, which results in a significant improvement of the quantitative precipitation forecast scores from MHS data assimilation. Details could be found in Zou et al. [10].

Continuous microwave humidity sounding data for more than 15 years had been provided by AMSU-B on board NOAA-15, -16, -17, MHS on aboard NOAA-18, -19, MetOp-A, MetOp-B, MWHS on aboard FY-3A, FY-3B, and ATMS on board Suomi NPP (as in Fig. 2). This unique dataset can be used for studying global climate change associated with water vapor information. For example, Moradi et al. [11] retrieved the tropospheric humidity profiles from microwave humidity observations from NOAA-15, -16, -18, -19 and MetOp-A, which were firstly compared with radiosonde data and then used for an investigation of the impact of water vapor in the middle and upper troposphere on global water cycle. Currently microwave humidity sounding data have not been widely used in climate research yet. With a continuous increase in time length of this dataset, however, microwave humidity sounders can be better utilized for global climate change studies related to water vapor.

参考文献/References

[1] Chen Y, Weng F, Han Y, et al. Validation of the Community Radiative Transfer Model by using CloudSat data. J Geophys Res, 2008, 113, D00A03.

[2] Guan L, Zou X, Weng F, et al. Assessments of FY-3A Microwave Humidity Sounder measurements using NOAA-18 Microwave Humidity Sounder. J Geophys Res, 2011, 116, D10106.

[3] Weng F, Zou X, Wang X, et al. Introduction to Suomi national polar-orbiting partnership advanced technology microwave sounder for numerical weather prediction and tropical cyclone applications. J Geophys Res, 2012, 117, D19112.

[4] Bonsignori R. The Microwave Humidity Sounder (MHS): In-orbit performance. Proc SPIE, 2007, 6744, 67440A.

[5] John V O, Holl G, Buehler S A, et al. Understanding intersatellite biases of microwave humidity sounders using global simultaneous nadir overpasses. J Geophys Res, 2012, 117, D02305.

[6] Weng F, Zou X. Errors from Rayleigh–Jeans approximation in satellite microwave radiometer calibration systems. Appl Opt, 2013, 52: 505-508.

[7] Li J, Zhu G F. Application analysis of direct assimilation of satellite radiation data on heavy rain forecasting. Meteorological Monthly, 2008, 34(12): 36-43.

[8] McNally A P, Anderson E, Kelly G. The use of raw TOVS/ATOVS radiances in the ECM WF 4D-Var assimilation system. Technical Proceedings of the 10th International ATOVS Study Conference, Boulder, Colorado, 27 January-2 February 1999.

[9] Qin Z, Zou X, Weng F. Evaluating added benefits of assimilating GOES imager radiance data in GSI for coastal QPFs. Mon Wea Rev, 2013, 141(1): 75-92.

[10] Zou X, Qin Z, Weng F. Improved quantitative precipitation forecasts by MHS radiance data assimilation with newly added cloud detection algorithm. Mon Wea Rev, 2013, 141: 3203-3221.

[11] Moradi I, Buehler S A, John V O, et al. Comparing upper tropospheric humidity data from microwave satellite instruments and tropical radiosondes. J Geophys Res, 2010, 115, D24310.